Plant Physiology and Biochemistry 206 (2024) 108296

Contents lists available at ScienceDirect

Plant Physiology and Biochemistry

journal homepage: www.elsevier.com/locate/plaphy

Ivermectin affects *Arabidopsis thaliana* microtubules through predicted binding site of β-tubulin

Yevhen Kustovskiy [a,b,*], Pavel Karpov [a], Yaroslav Blume [a], Alla Yemets [a,b]

[a] Institute of Food Biotechnology and Genomics, National Academy of Sciences of Ukraine, Baidy-Vyshnevetskoho str., 2a, Kyiv, 04123, Ukraine
[b] National University of Kyiv-Mohyla Academy, Skovorody str., 2, Kyiv, 04070, Ukraine

ARTICLE INFO

Handling Editor: Shivendra Sahi

Keywords:
Ivermectin
Arabidopsis thaliana
Haemonchus contortus
Microtubules
β-tubulin
Binding site
In silico
Spatial reconstruction

ABSTRACT

The ivermectin is a potent nematocide and insecticide, which has low toxicity for humans and domestic animals, but due to low biotransformation, it can be dangerous for non-target organisms. The recent determination of ivermectin absorption and accumulation in tissues of higher plants and multiple shreds of evidence of its negative impact on plant physiology provide a basis for the search for ivermectin's molecular targets and mechanisms of action in plant cells. In this research, for the first time, the ivermectin effect on microtubules of *Arabidopsis thaliana* cells was studied. It was revealed that ivermectin (250 μg mL^{-1}) disrupts the microtubule network, induces the loss of microtubule orientation, leads to microtubule curvature and shrinkage, and their longitudinal and cross-linked bundling in various cells of *A. thaliana* primary roots. Further, the previously proposed binding of ivermectin to the β1-tubulin taxane site was developed and confirmed using molecular dynamics simulations of ivermectin complexes with *Haemonchus contortus* and *A. thaliana* β1-tubulins. It was predicted that similar to other microtubule stabilizing agents ivermectin binding causes M-loop stabilization in both *H. contortus* and *A. thaliana* β-tubulin, which leads to the enhancement of lateral contacts between subunits of adjacent protofilaments preventing microtubule depolymerization.

1. Introduction

The antiparasitic ivermectin (22, 23-dihydroavermectin B1; further referred to as IVM) is an endectocide with potent nematocide and insecticidal activity, which is used in veterinary and human medicine (Laing et al., 2017). Due to a wide range of earlier determined molecular targets (Chen and Kubo, 2018; Martin et al., 2020), IVM is considered a broad-spectrum drug. Since its pharmacokinetics in domestic animals is characterized by low metabolism, more than 90% of the administrated doses of IVM are excreted unchanged with faeces (González Canga et al., 2009). Similarly to many drugs, when released into the environment, it may have negative effects on non-target organisms, including plants. The determination of IVM absorption and accumulation in plant tissues by Iglesias et al. (2018) laid the foundation for the research of IVM toxicity for higher plants (Syslová et al., 2019; Vokřál et al., 2019; Langhansová et al., 2021; Navrátilová et al., 2020). In particular, inhibition of root growth at nanomolar concentrations of IVM was reported by Vokřál et al. (2019) for *Sinapis alba* seedlings. Although no negative effect on *Arabidopsis thaliana* growth was observed by Syslová et al. (2019) after the treatment with IVM in low micromolar concentrations, significant transcriptomic changes in roots and rosettes were reported, which mainly included activity of genes involved in response to various types of stress. In the papers by Navrátilová et al. (2020 ab), IVM influence on the activity of ROS-controlling enzymes and the secondary metabolites content in *Plantago lanceolate* and *Glycine* max was reported. Changes in the activity of ROS-protecting enzymes of *Trifolium pratens* after the IVM treatment were reported by Langhansová et al. (2021).

Despite this evidence of IVM impact on plant physiology, no molecular targets have been identified so far and no mechanism of IVM action in plant cells has been determined. In a recent article de Souza et al. (2022) reported that eprinomectin, a structurally related to IVM member of the avermectin family, has an aneugenic mode of action in meristematic cells of *Allium cepa*, which can be related to the disruption of spindle formation. This suggestion is based on the facts of IVM influence on the expression of dyneins and kinesins (motor proteins associated with microtubules, MTs) of *Caenorhabditis elegans* (Ballesteros

* Corresponding author. Institute of Food Biotechnology and Genomics, National Academy of Sciences of Ukraine, Baidy-Vyshnevetskoho str., 2a, Kyiv, 04123, Ukraine.
E-mail addresses: kustovskyi_yo@nas.gov.ua (Y. Kustovskiy), karpov.p.a@gmail.com (P. Karpov), blume.yaroslav@nas.gov.ua (Y. Blume), yemets.alla@nas.gov.ua (A. Yemets).

https://doi.org/10.1016/j.plaphy.2023.108296
Received 31 August 2023; Received in revised form 5 December 2023; Accepted 18 December 2023
Available online 19 December 2023

et al., 2016), IVM-induced single nucleotide polymorphisms in β-tubulin sequences of *Onhocerca volvulus* and *Haemonhus contortus* (Eng et al., 2006), and IVM stabilizing effect on the MTs of *H. contortus* were reported by Ashraf et al. (2015a, 2015b). According to these reports, the IVM and moxidectin, another macrocyclic lactone belonging to the milbemycin family, both directly bind to the taxane site of *H. contortus* β1-tubulin and have similar to taxol stabilizing effect on MTs, which can subsequently lead to antimitotic activity and cell cycle arrest. Considering that the molecular dynamics of IVM interactions with tubulin of plant origin and the IVM influence on plant MTs have not been studied yet, this research aimed to study the IVM effect on *A. thaliana* MTs, and to develop and verify the shreds of evidence for IVM binding to the taxane site of β-tubulin, which was proposed by Ashraf et al. (2015a, 2015b). In this regard, the dynamic properties of the IVM complex with *H. contortus* tubulin were studied and compared with those of the complex of IVM with *A. thaliana* tubulin, providing important structural information about IVM-tubulin interactions and structure-activity relationships (SAR) of IVM-tubulin complexes. Finally, IVM's influence on the growth of *A. thaliana* seedlings was investigated and explained given its effect on *A. thaliana* MTs.

2. Materials and methods

2.1. Chemicals and reagents

IVM (Product No. I8898), which is a mixture of B1a (>90%) and B1b (<10%) components (Martin et al., 2020), and Murashige and Skoog basal medium (MS; Product No. M5519) were purchased from Sigma-Aldrich (USA). IVM was dissolved in dimethyl-sulphoxide (DMSO) and used at 50, 100, 250 and 500 μg mL^{-1} concentrations. Stock solution of IVM (10 mg mL^{-1}) was stored under at 2–8 °C in the dark as recommended.

2.2. Plant materials and growth conditions

A. thaliana (L). Heynh. ecotype Columbia (Col-1) (wild type, WT), *A. thaliana* ecotype Landsberg erecta (Ler-0) expressing fused gene *gfp-map4* (microtubule-associated protein 4) (Marc et al., 1998; Mathur and Chua, 2000), and *A. thaliana* expressing fused gene *gfp-tua6* (Ueda et al., 1999) were used to study the influence of IVM on *A. thaliana* growth *in vitro* and on MT organization in living cells. Seeds of these lines were obtained from the Nottingham Arabidopsis Stock Centre (NASC, UK). To perform *in vitro* experiments *A. thaliana* seeds were sterilized, and stratified, and seedlings were grown as described by us earlier (Blume et al., 2010, 2013). The sterilization protocol included treatment of seeds with 50% (v/v) sodium hypochlorite for 10 min followed by five cycles of sterile water rinsing, after which seeds were planted on MS medium supplemented with 3% (w/v) sucrose, 0.4% (w/v) agar, pH 5.7. Petri dishes were placed vertically in a growth chamber where seeds germinated and seedlings were grown at 23 °C and 8 h dark/16 h light photoperiod.

2.3. Study the effect of IVM on A. thaliana growth and development

For an *in vitro* study, sterilized *A. thaliana* seeds were planted on the surface of MS medium supplemented with IVM in tested concentrations for germination and further seedling development in a growth chamber for 12 days. The changes in seedlings' growth in the presence of IVM were investigated in 3, 6, and 12 days. Time-lapse images of growing *A. thaliana* seedlings *in vitro* were captured by a Canon Power Shot G6 digital camera (Canon, Taiwan) in the macro mode. The growth parameters were measured with Image J software version (2.9.0) (Schindelin et al., 2012) freely available on the site http://rsb.info.nih.gov/ij/.

Experiments were repeated at least three times with up to 30 seedlings for each concentration/time point.

2.4. Confocal laser scanning microscopy

The confocal laser scanning microscope CLSM 510 META (Carl Zeiss, Jena, Germany) equipped with the Differential Interference Contrast (DIC) was used to study the IVM effects on MTs of *A. thaliana* primary root cells. For this, six-day-old seedlings of the *A. thaliana* transgenic lines (expressing *gfp-map4* and *gfp-tua6*) were treated with IVM in concentrations of 50, 100, and 250 μg mL^{-1} for 1 and 2 h. Distilled water and DMSO were used for the treatment of *A. thaliana* as controls.

To study the organization of MTs in root cells the fluorescent signal from GFP fused protein was visualized with a confocal microscope using the Plan-Apochromat 63x/1.4 Oil DIC objective, excitation 488/543 nm, emission 505/530 nm) and scanned unidirectionally in the frame mode with 100–300 nm step along z-axis. The resulting stacks containing frames of 1024 × 1024 size and technical information were accessed in FIJI using the LSM Toolbox plugin v. 4.1.2 and projected along the z-axis for analysis. Orientations of MTs in treated and untreated cells were determined in FIJI with the Fourier components analysis method of the Directionality plugin (Sasaki et al., 2017).

Experiments were set in triplicate; in each experiment, at least 30 seedlings of each *A. thaliana* line were used per concentration/timepoint.

2.5. 3-D modelling of tubulin structure

The theoretical models of eight isotypes of *A. thaliana* β-tubulin (UniProt accessions: P12411, Q56YW9, P24636, P29513, P29514, P29515, P29516, P29517) and *H. contortus* β1-tubulin (A2TF56) predicted with the AlphaFold Monomer v. 2.0 pipeline and deposited in the AlphaFold Protein Structure Database were retrieved from UniProtKB (Jumper et al., 2021). Before application of molecular docking and molecular dynamics methods, structures and their sequences were compared in the free version of Maestro v. 13.1 (Schrödinger Release, 2022-1, 2022). Further, residues of taxane site secondary structure were selected in the alignment and compared in terms of their identity, similarity, and conservation. Images of the resulting alignment were made using Jalview v. 2.11.2.6 (Waterhouse et al., 2009).

2.6. The molecular dynamics setup

The simulations were performed using the GROMACS v. 2022.4 (https://www.gromacs.org) compiled in mixed precision with CUDA support for GPU acceleration (Abraham et al., 2015). In simulations, the all-atom additive CHARMM36 force field was used with the recommended TIP3P water model implemented as an explicit solvent (Huang and MacKerell, 2013). The Particle Mesh Ewald (PME) method was used for the

calculations of electrostatic interactions with parameters set as recommended for simulations with CHARMM36 force field (Darden et al., 1993). Similarly, the recommended plain cutoff of 1.2 nm was used for the calculations of van der Waals forces. Only bonds to hydrogens were constrained using the single-step LINCS algorithm with the order of 4. The periodic boundaries of systems were defined using the dodecahedral box with the minimum solute-wall distance of 1 nm. To reproduce physiological conditions molecules of solvent and ions (Na^+/Cl^-) were added to the systems with the tubulins and tubulin-IVM complexes in its center. The obtained systems with a total neutral charge were further minimized using the steepest descent algorithm and equilibrated for 200 ps with the establishment of NVT and NPT ensembles. During both equilibration and productive run the thermal bath coupling with the temperature of 300 K was performed separately for solid-state (free or IVM-bound tubulins) and liquid-state (water and ions) of the systems using the V-rescale thermostat. The C-rescale barostat was used to reach the pressure of 100 kPa (1 bar) on the NPT stage of equilibration. Equilibrated systems were used for the production runs, during which the Parinello-Rahman barostat was implemented for pressure coupling. All runs were performed with the 2 fs step of the leap-frog time integrator; energies and centre of mass motions were calculated every 100 ps; coordinates were stored uncompressed every 10 ps.

2.7. The protocol of molecular docking

The IVM B1a (IVM; PDB: IVM, PubChem: 6321424) structure was obtained from the complex of IVM bound to *Caenorhabditis elegans* glutamate-gated Cl^- channel GluCl) deposited in PDB (entry 3RI5). The structure quality was accessed in SeeSAR (SeeSAR version 12.1.0, 2023), where it was reprotonated and its connect records were reassigned, and in GOLD v. 5.3 suite of programs before docking (Jones et al., 1997). The full atom IVM model containing 62 heavy atoms and 74 hydrogens was minimized in vacuum before docking. The semi-flexible molecular docking of IVM to the taxane sites of *A. thaliana* and *H. contortus* β1-tubulin was performed using the CCDC GOLD suite. As the main scoring function, the default GOLD empirical ChemPLP function was used, and the ASP function was used for rescoring (Mooij and Verdonk, 2005; Korb et al., 2009). The 100 runs of genetic algorithm for each target were performed with a search efficiency of 200% and all the produced solutions were saved for subsequent analysis. Best solutions were selected based on GOLD scoring and examined in the Analyzer Mode of SeeSAR. The affinities and h-bond networks of the protein-ligand complexes were accessed using the HYDE scoring, which is discussed in the paper by Schneider et al. (2013). Based on the results of analysis the best solutions for each IVM-tubulin complex were chosen for molecular dynamics (MD).

2.8. The modelling of IVM-tubulin interaction

Considering the high conservation of *A. thaliana* β-tubulin isotypes, only the β1-tubulin, which is expressed in *A. thaliana* roots, was chosen for molecular docking and molecular dynamics. The 1 isotype of *H. contortus* β-tubulin, which was previously used in the research by Ashraf et al. (2015a,b), was chosen to compare IVM-induced conformational changes of *H. contortus* and *A. thaliana* β-tubulin. Initially, the 100 ns simulations of *A. thaliana* and *H. contortus* β1-tubulin were performed to collect the conformational ensembles of the targets. An equilibrated state of the protein was determined based on the results of RMSD, h-bonds, and polar contacts calculations performed using programs of GROMACS suite and salt bridge calculations performed in visual MD (Humphrey et al., 1996). Frames corresponding to the equilibrated state were derived from the trajectories and analyzed manually in the Binding Site Mode of SeeSAR, which pocket detection algorithms are based on the DoGSiteScorer (Volkamer et al., 2010, 2012). To determine the most common conformations of *A. thaliana* and *H. contortus* β1-tubulin taxane sites, clustering was performed for the index group of site-forming residues using the gromos method with 0.1 nm cutoff (Daura et al., 1999). The middle structures of the most populated clusters with opened conformations of taxane sites were derived from the trajectories and analyzed. The IVM conformations obtained from docking were parametrized for CHARMM forcefield using the SwissParam server (Zoete et al., 2011) and the stability of complexes was verified using MD. The h-bonds and polar contacts of the resulting trajectories were analyzed and interpreted given IVM-induced conformational changes of tubulin. The conformations of the IVM-bound taxane site of *A. thaliana* and *H. contortus* β1-tubulins collected from the stabilized part of the MD trajectory were clustered using the same method and cutoff as described above. The middle structures of each cluster of IVM-tubulin complexes were visualized and analyzed in the Analyzer Mode of SeeSAR. Considering the crucial role of M-loop in the mechanism of MT stabilization by taxane site binding agents, its conformational ensemble in IVM-bound and unbound state of *A. thaliana* and *H. contortus* β1-tubulin taxane sites was studied and compared using clustering and RMSF calculations.

Molecular dynamics calculation was carried out with the assistance of The Ukrainian National Grid (UNG) (http://grid.nas.gov.ua) and the IFBG cluster of the virtual organization CSLabGrid (Karpov et al., 2015).

2.9. Statistical analysis

The data collected from *in vivo* and *in vitro* experiments were processed in Excel (2016) using the one-way ANOVA ($\alpha = 0.05$). To determine the statistical significance of differences between unequal mean group values, the post hoc Tukey-Kramer test was performed. The outputs of analyzing modules of the GROMACS suite and VMD plugins were exported to Excel for final data processing and graph creation.

3. Results

3.1. Effect of IVM on A. thaliana growth and development

The influence of IVM on the growth and development of *A. thaliana* seedlings was investigated on the 3rd, 6th, and 12th days of the study. The main morphological parameters of the seedlings were also evaluated, with a special focus on root development. It should be noted that after 3 days of the study, we did not observe pronounced disturbances in seed germination or noticeable disturbances in morphology of *A. thaliana* seedlings. However, after 6 and especially after 12 days, disturbances in the morphology of the roots, which grew in the presence of IVM at 250 and 500 μg mL^{-1} concentrations, were observed. The roots

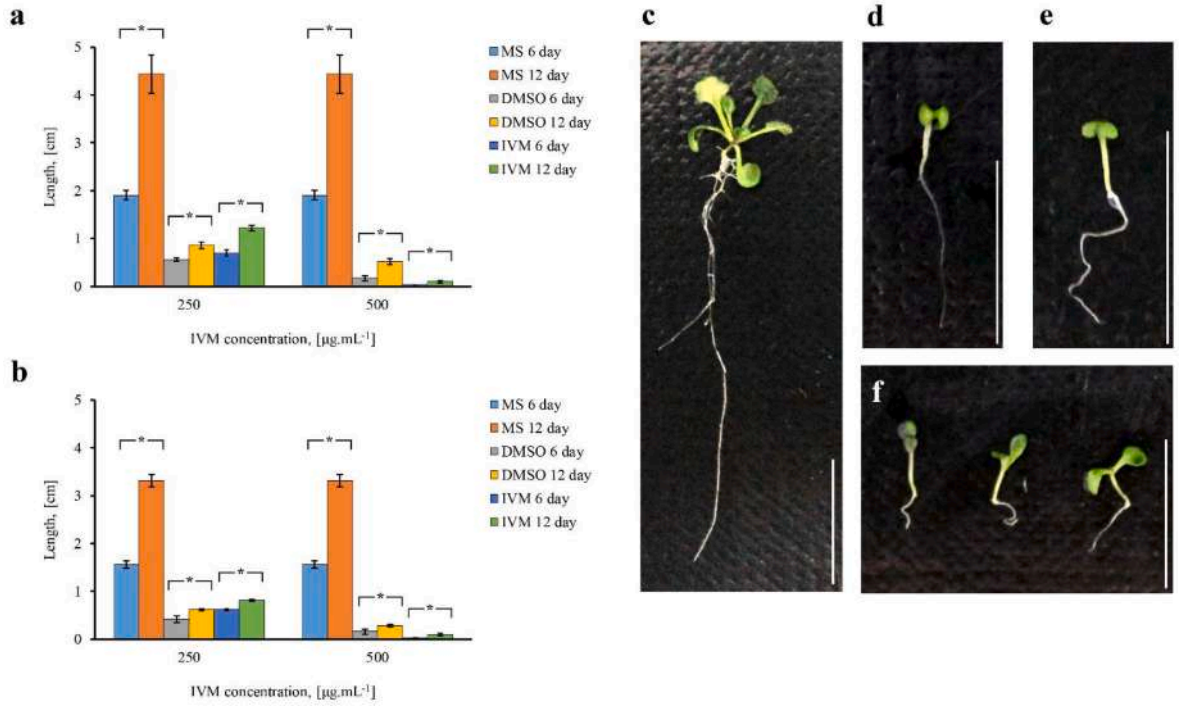

Fig. 1. The IVM influence on growth and development of *A. thaliana* seedlings. The length of *A. thaliana* seedlings (a) and roots (b) after 6 and 12 days of cultivation in the presence of 250 and 500 μg mL^{-1} IVM.

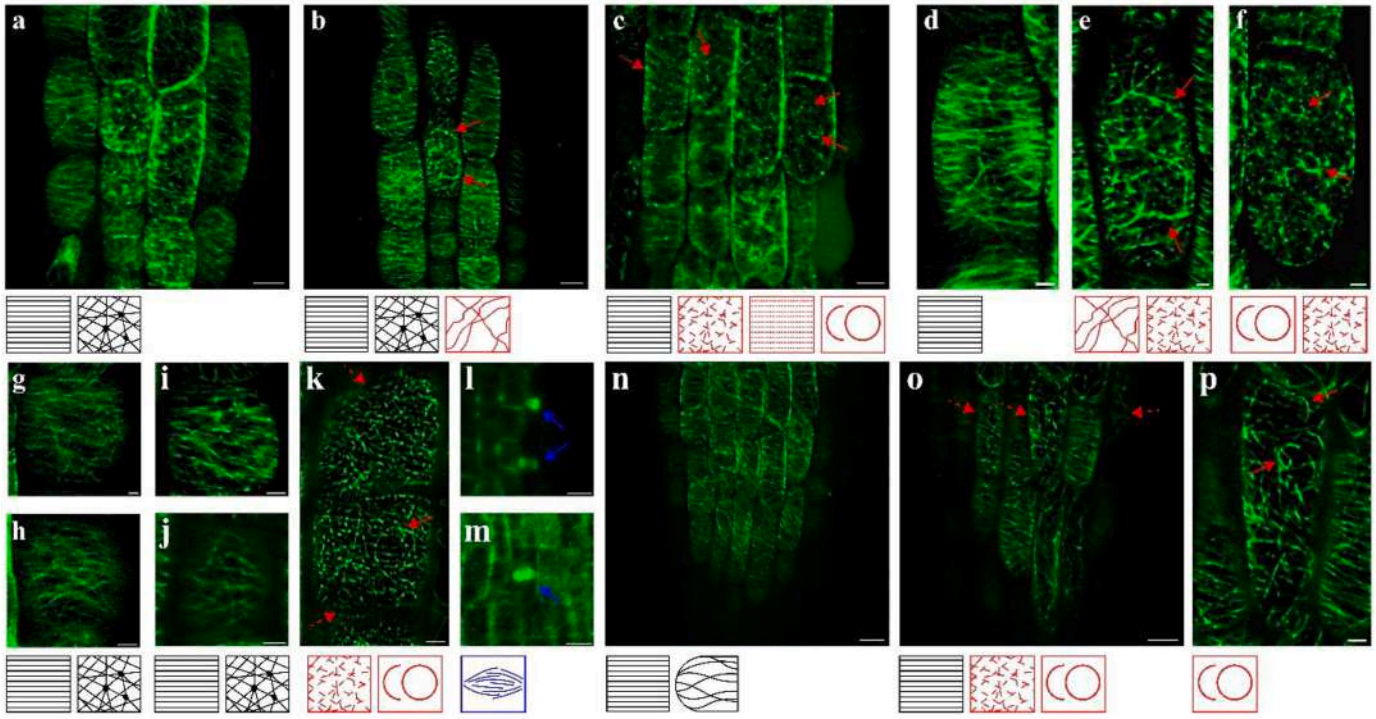

Fig. 2. IVM influence on the MTs of *A. thaliana gfp-map4* cells of root apex, meristematic cell division and transition zones. Control (a, d, g, h, l, n): (a, d) transition zone; (g, h) meristem cell division zone; (n) root apex. (b, e, i, j) DMSO (2.5% 1h): (b, e) transition zone; (i, j) meristem cell division zone. (c, f, k, m, o, p) IVM (250 μg mL^{-1} 1h): (c, f) transition zone; (k, m) meristem cell division zone; (o, p) root apex. Bar = 10 μm (a-c, l-o); 3 μm (d-k, p).

were shortened, and curved, with short underdeveloped root hairs; with an increase in IVM concentration to 500 μg mL^{-1}, root hairs practically did not form on *A. thaliana* primary roots. As opposed to seedlings in control, which had branched root systems on the 12th day of the cultivation (Fig. 1c), secondary roots only started to develop in seedlings exposed to 250 μg mL^{-1} concentration of IVM (Fig. 1d). Moreover, no secondary root development was observed in seedlings cultivated on a medium containing 500 μg mL^{-1} IVM on the 12th day.

Statistically significant differences between groups revealed by the post hoc Tuckey-Kramer test are marked with asterisks (*). Macroscopic images of *A. thaliana* seedlings on the 12th day of cultivation: (c) MS; (d) 250 μg mL^{-1} IVM; (e) DMSO 2.5%; (f) DMSO 5.0%; seedlings which grew on medium with 500 μg mL^{-1} IVM are not represented due to near zero length. Scale bar = 1 cm.

The statistically significant differences in growth parameters of *A. thaliana* seedlings cultivated *in vitro* in the presence of IVM and on a control medium were revealed on the 6th and 12th day of cultivation. In particular, it was determined that the lengths of seedlings and their primary roots, which grew on medium with IVM or DMSO, decreased considerably compared to control (Fig. 1a and b). Although seedlings cultivated on medium containing 250 μg mL^{-1} IVM were longer than seedlings, which grew on DMSO-supplemented medium, at the IVM concentration of 500 μg mL^{-1} almost total inhibition of seedlings growth was observed on the 12th day of cultivation. As demonstrated in Fig. 1b, the most significant inhibition at this concentration was observed for the roots of seedlings supporting the observed changes in their morphology. Since similar changes in morphology and growth parameters were also observed in seedlings grown on a medium containing DMSO as positive control they are not restricted to IVM action. However, the most significant changes were observed in roots, which grew in the presence of 500 μg mL^{-1} IVM, we conclude that IVM has an inhibiting effect on the growth and development of *A. thaliana*.

3.2. Influence of IVM on microtubules of A. thaliana primary root cells

The effect of IVM on plant MTs was analyzed in living cells of different root zones of both *A. thaliana gfp-map4* and *A. thaliana gfp-tua6* lines. We first studied the effects of IVM on MTs of cells of the root apex, meristem, transition and elongation zones of primary roots of the *A. thaliana gfp-map4* line. The effect of 250 μg mL^{-1} (1 h treatment) was especially visible for epidermal cells of the elongation zone, which have a transverse orientation of cortical MTs in control seedlings (Fig. 2d,n; Fig. 3a,e).

During these rearrangements in cells of the elongation zone, which normally have transverse orientations of cortical MTs (Fig. 3b), the loss of MT orientations and their translocations were observed. The DMSO-treated cells lacked curved MTs, their bundles, and ring-shaped assemblies that appeared after IVM treatment. No significant effect on the MT arrangements was observed in root cells of the differentiation zone after IVM or DMSO treatment (Fig. 3h,i,k-m).

Comparisons of MT orientation in untreated and IVM-treated cells were performed for the zones in which the IVM effect was most prominent, i.e., root apex, transition zone and elongation zone, to obtain a quantitative description of IVM-induced changes in MT organization. As it is demonstrated in Fig. 4, most of the MTs in control cells have angles within the range of -30–30° and thus are close to the ideal transverse orientation (0°). On the contrary, in IVM-treated cells, loss of MT orientations is observed leading to an almost uniform distribution of MTs among all angle groups. Moreover, the disruption of MT arrangements and loss of MT orientations are the most prominent for elongation zone cells due to the smoothness of MT distributions (Fig. 4a, d).

The amounts of MTs in the given directions are represented on the graphs: (b) root apex cells; (c) transition zone cells; and (d) elongation zone cells. Bar = 10 μm.

The observations of the IVM effect on MT organization in cells of the *A. thaliana gfp-map4* line were verified with an additional study on the *A. thaliana gfp-tua6* line. Similarly to the *A. thaliana gfp-map4* line, after 1 h of treatment with 250 μg mL^{-1} IVM, its effect on MT arrangements was observed in cells of root apex (Fig. 5b and c), which included disruption of MT organization, loss of MT orientations (typically transverse for cells of root apex; e.g., Fig. 5a), and MT assembling into thick bundles with more intense emission. Finally, through the comparison of MT orientations in untreated and IVM-treated cells loss of MT orientations was confirmed quantitatively (Fig. 5d).

3.3. Comparison of β-tubulin taxane sites of A. thaliana and H. contortus

Given that IVM was previously found to compete with taxol for the same binding site in *H. contortus* β-tubulin (Ashraf et al., 2015a, 2015b), a comparative analysis of the taxane sites of β-tubulin isotypes of *A. thaliana* and *H. contortus* was carried out. According to the results of Multiple Sequence Alignment (MSA) (Fig. 6), *A. thaliana* β1-and β5-tubulin contain insertion of alanine (Ala) in the position 41 as opposed to other isotypes of *A. thaliana* and *H. contortus* β1-tubulin. Although this insertion does not influence the taxane site conservation, it leads to a shift in indexes of the subsequent residues. Therefore, in the description of SAR of IVM complexes with *A. thaliana* and *H. contortus* β1-tubulin the *H. contortus* residue index is given in the parenthesis near the index of respective residue of *A. thaliana*.

Sequences of *A. thaliana* β-tubulin isotypes in taxane site, share on average 90% of conservation with the sequence of *H. contortus* β1-tubulin. Among these regions, unstable elements (H6–H7, M-loop, and S9–S10) are the least conserved. In particular, the M-loop differs in positions 275–277 (274–276), 279 (278), 281 (280), and 283–286 (282–285). On the contrary, the stable elements of the structure (H1, H6, H7 and part of S7) have almost no significant differences.

3.4. IVM interaction with A. thaliana and H. contortus β1-tubulin

The middle structures of MD-clusters of IVM-tubulin complexes were derived from trajectories and analyzed. Based on the results of the HYDE assessment, these structures demonstrate the positive contribution of 16-membered lactone ring and spiroketal group to complexes affinities in desolvation energies of binding (Fig. 7). Particularly, the lactone ring is deeply inserted into the first cavity of taxane site interface and is surrounded by mainly hydrophobic residues Leu216(215) of H6; Leu229 (228) and Val232(231) of H7; Pro273(272) of S7; Leu274(273), Thr275 (S274), and Q280(279) of M-loop. Similarly, the spiroketal group interacts with R277(K276), Gln280(279), and Gln281(Ala280) of M-loop; Thr360(359) and Gly361(360) of S9–S10.

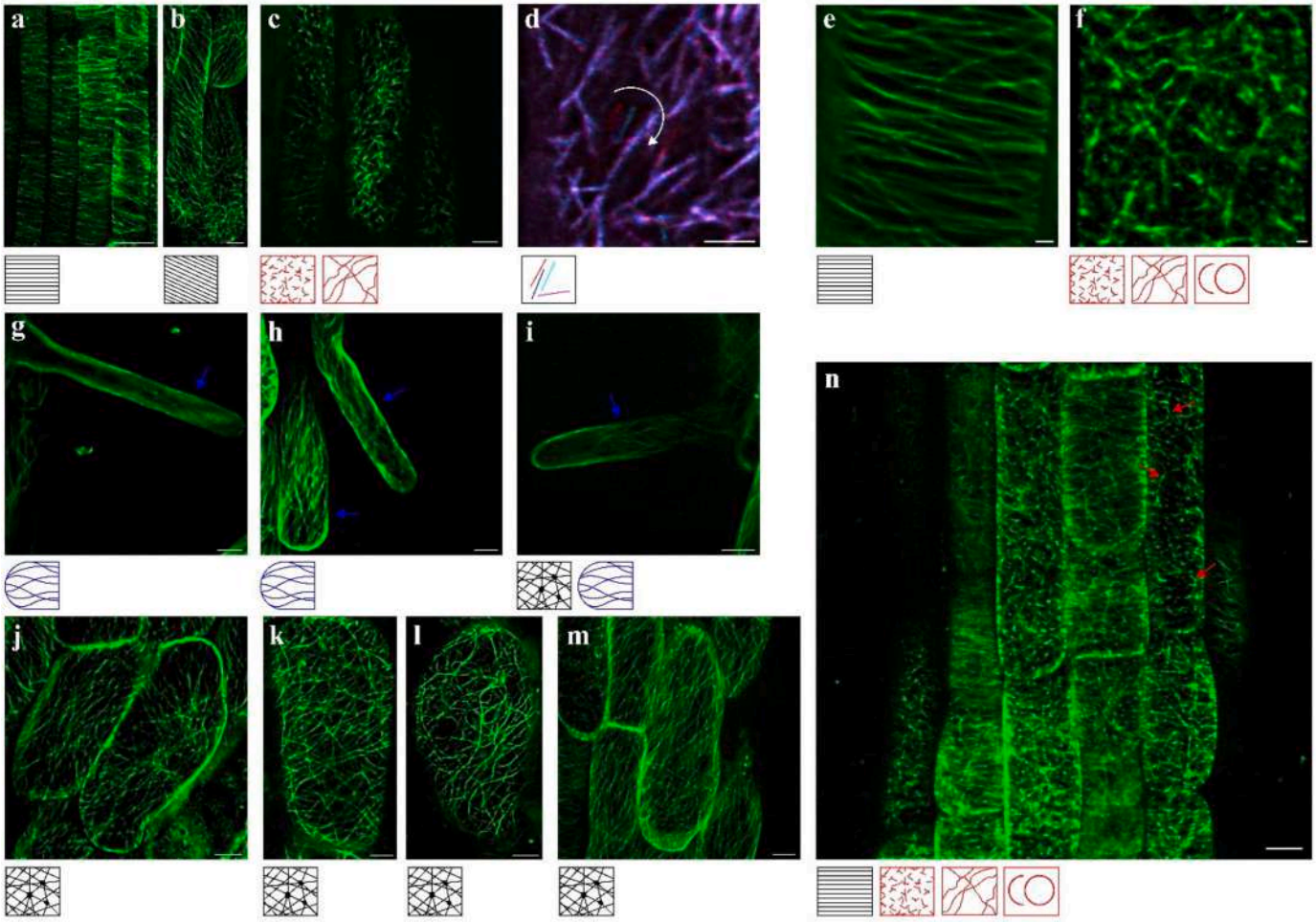

Fig. 3. IVM influence on the MTs of *A. thaliana gfp-map4* elongation and differentiation zone cells. MS (a, b, e, g, j): (a, b, e) elongation zone; (g) root hair; (j) differentiation zone. (c, d, h, k, l) DMSO (2.5% 1,2 h): (c, d) elongation zone (2 h); (h) root hair (1 h); (k, l) differentiation zone (1, 2 h respectively). (f, i, m, n) IVM (250 μg mL^{-1} 1h): (f) elongation zone; (i) root hair; (m) differentiation zone; (n) elongation zone. Bar = 10 μm (a-c, g-n); 3 μm (e, f).

The trajectories were analyzed to determine the most persistent hydrogen bonds and to describe the hydrogen bond networks of complexes (Fig. 8). In each trajectory, only one hydrogen bond to the spiroketal group between the oxygen of its first ring and Arg277 (*A. thaliana*) or Gln279 (*H. contortus*) was determined, which in both cases have low persistence. Despite the non-stable h-bond between the oxygen of the carbonyl group and Arg360 (Thr359), contacts of the lactone ring ester segment with Gly361(360), and Ile362(Leu361) of S9–S10 harm the affinity of both complexes according to HYDE. The spiroketal group has a higher affinity for *H. contortus* tubulin, which is related to the side chain of Arg277 of *A. thaliana* β1-tubulin preventing the spiroketal group's deeper insertion into the taxane site pocket. The donor hydroxyl groups make disaccharide (1 group) and benzofuran (2 groups) centres of h-bond networks. According to the developed model of binding, the benzofuran is located in the second cavity of the taxane site and is surrounded by residues of H1 (Val23, Asp26, Glu27), H7, and S9–S10. The hydroxyl group connected to cyclohexene ring of benzofuran significantly contribute to complex affinity through the establishment of h-bonds with Glu27 (OE1, OE2, and N), Val23 (N) and Asp26 (OD1); another hydroxyl group of benzofuran has h-bonds with NE2 of His228(H227) and OG of Ser231 (in *A. thaliana* tubulin only). The number of h-bonds with disaccharide is higher for β1-tubulin of *H. contortus*, but the network with disaccharide as its centre is prominent for both complexes: in these interactions, Arg277 (Lys276) and Lys19 are donors and Asp225(224) is the acceptor. While His228(227) is a donor in complex with *A. thaliana* β1-tubulin, it acts as both donor and acceptor in complex with *H. contortus* one (Fig. 8). Therefore, unlike macrocycle and spiroketal groups, which have mainly hydrophobic interactions, a benzofuran and disaccharide form multiple polar contacts and h-bonds with the above-mentioned residues.

Finally, the IVM influence on the M-loop was studied. The low identity of sequences of *A. thaliana* and *H. contortus* β1-tubulin M-loops mentioned in the previous section leads to different conformational properties. In particular, the *H. contortus* M-loop is more flexible compared to the *A. thaliana* one, which results in a considerable increment in the total number of clusters demonstrated on the graphs (Fig. 9 a,e). Although the IVM binding stabilizes the M-loop conformation of both structures, its stabilization is more pronounced for *A. thaliana*, which is generally less flexible (Fig. 9 b,f). Also, no correlation was observed between IVM h-bonds (blue marks) and polar contacts (green marks) established with residues of M-loop and its stabilizing effect on M-loop conformation in both *A. thaliana* and *H. contortus* β1-tubulin.

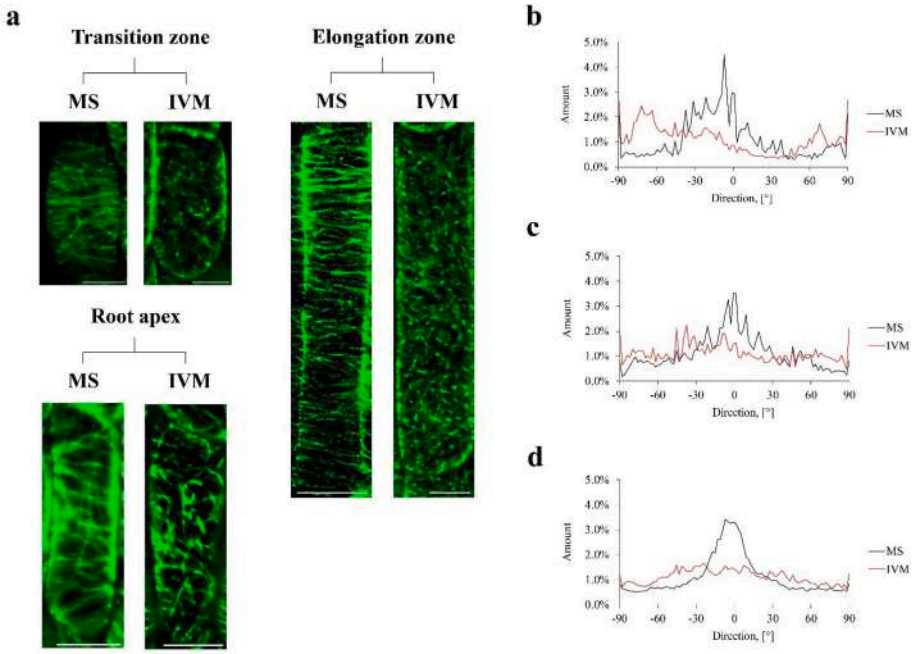

Fig. 4. The comparison of MT patterns in IVM treated (250 μg mL^{-1}, 1h) and untreated cells of *A. thaliana gfp-map4* line: (a) cells of root apex, transition, and elongation zone. The amounts of MTs in the given directions are represented on the graphs: (b) root apex cells; (c) transition zone cells; and (d) elongation zone cells. Bar = 10 μm.

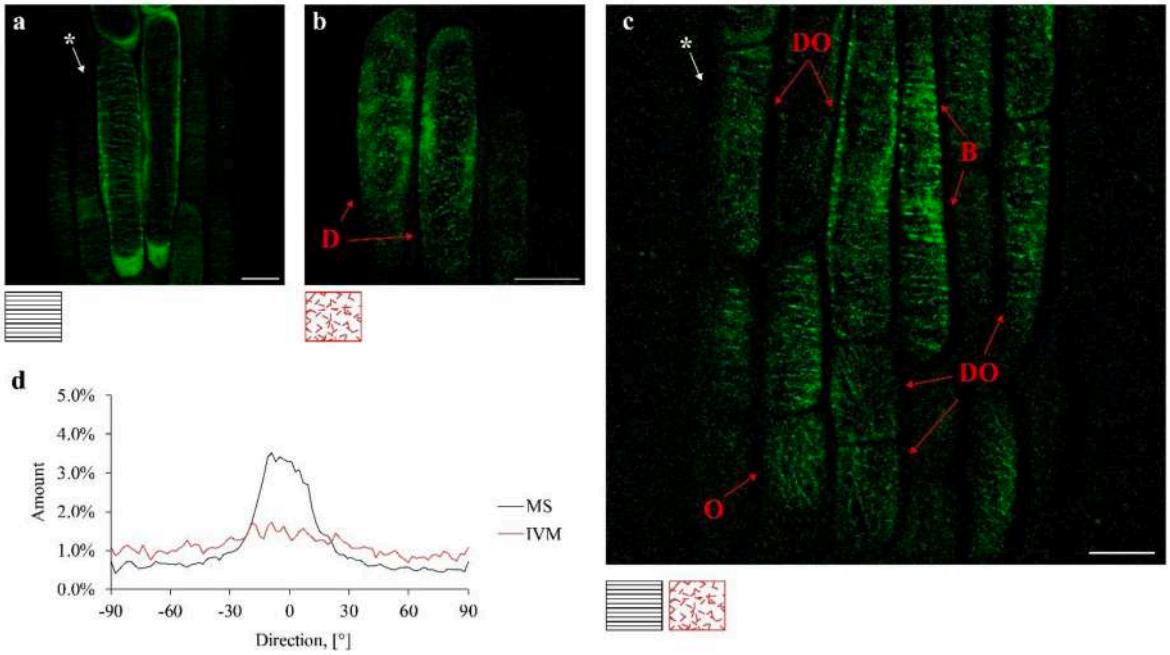

Fig. 5. IVM influence on MTs of the root apex of *A. thaliana gfp-tua6* line: (a) control; (b,c) IVM (250 μg mL^{-1} 1h); (d) comparison of MT orientations in control cells and IVM-treated cells with disrupted MT arrangements (cells which were used for comparison are marked with asterisks). In the images of IVM-treated cells (b, c) following markers are used to highlight the IVM effect: B for MT bundling; D – disruption of MT arrangements; O – change in MT orientation. Bar = 10 μm.

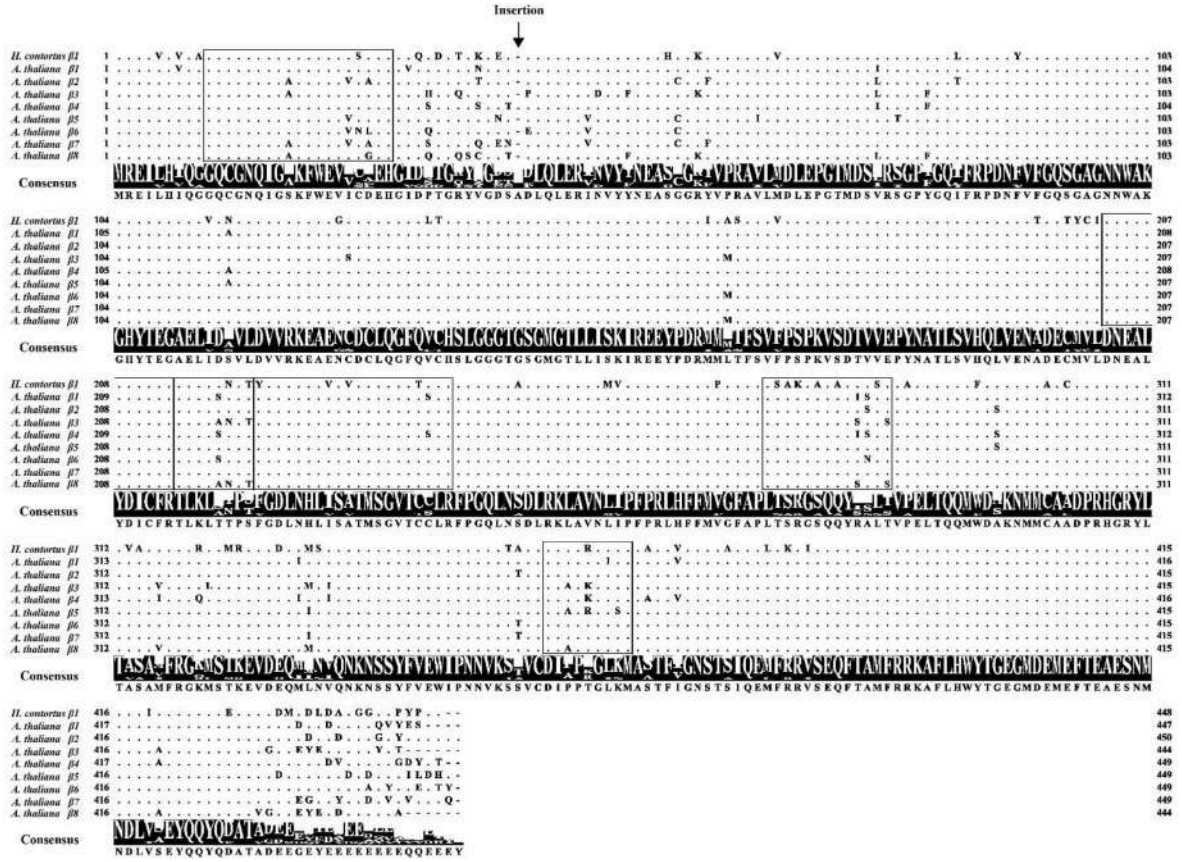

Fig. 6. The MSA of eight *A. thaliana* β-tubulin isotypes and *H. contortus* β1-isotype. Regions of the taxane site secondary structure (i.e., H1, H6, H6–H7, H7, S7, M-loop, and S9–S10) are highlighted with borders.

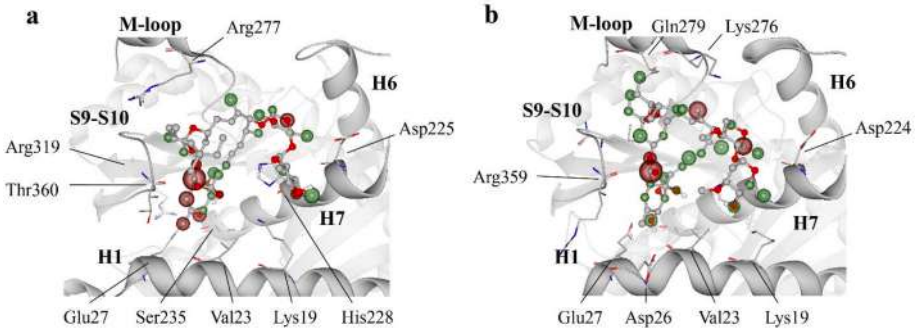

Fig. 7. The middle structures of major clusters of IVM-bound (a) *A. thaliana* and (c) *H. contortus* β1-tubulin taxane sites. Only residues involved in tubulin-IVM h-bonds networks are visualized. The positive or negative contributions of IVM heavy atoms to complex affinity are highlighted with HYDE colouring.

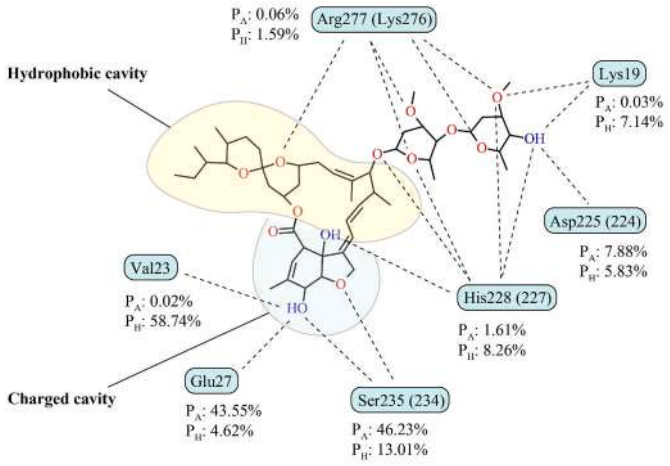

Fig. 8. The scheme describing most persistent hydrogen bonds of the trajectories common for *A. thaliana* (P_A) and *H. contortus* (P_H) β1-tubulin.

4. Discussion

Having studied the effects of IVM in different concentrations, we have shown that 50–100 μg mL^{-1} IVM does not have any toxic effect on seed germination, growth and morphology of seedlings of the analyzed *A. thaliana* lines. However, during long-term cultivation of seedlings in the presence of 250 μg mL^{-1} IVM, delays in their growth and development, as well as morphological changes in the roots, were observed. The most toxic concentration of IVM was 500 μg mL^{-1}, in the presence of which seedlings could not grow and develop (Fig. 1). Similar growth delays were observed for seedlings grown on media containing 2.5 and 5% DMSO, indicating that high concentrations of DMSO are phytotoxic. However, these changes were different from those induced by IVM. For instance, 250 μg mL^{-1} IVM slightly stimulated the growth of seedlings compared to DMSO (Fig. 1a,b,d,e); on the contrary, at 500 μg mL^{-1} IVM, virtually no growth was observed (Fig. 1a and b), whereas on medium with 5% DMSO weak growth and development were noticed (Fig. 1a, b, f). The stimulating effect of 250 μg mL^{-1} IVM can be explained by IVM-induced changes in the expression of certain genes, which were recently reported by Syslová et al. (2019) for *A. thaliana*. Although the studied

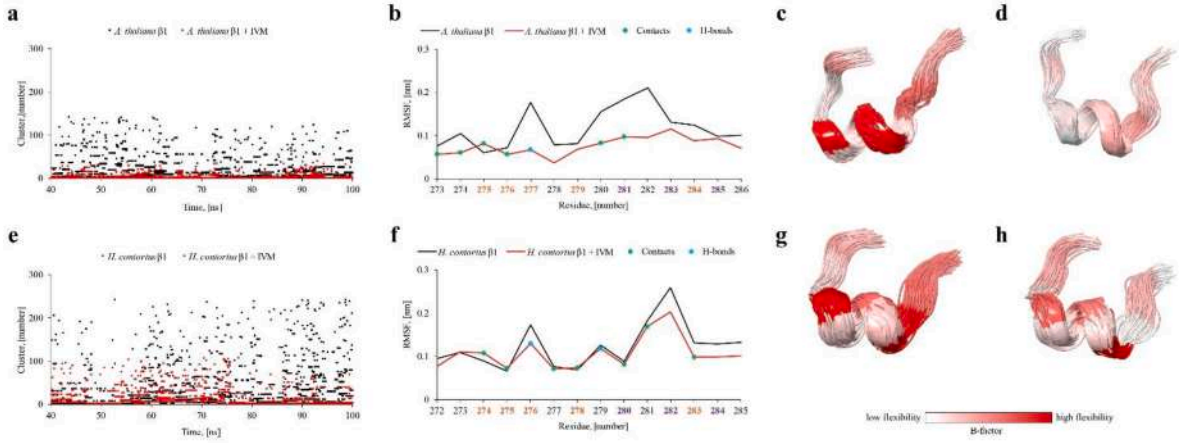

Fig. 9. The IVM influence on M-loop conformation. The comparison of M-loop clusters number of unbound and IVM-bound taxane sites of (a) *A. thaliana* and (e) *H. contortus* β1-tubulin. The RMSF of M-loop residues (IVM interactions with residues are marked with green for contacts and blue for h-bonds; substitutions for similar residues are highlighted with orange, non-similar with violet): (b) *A. thaliana*; (f) *H. contortus*. The middle structures of M-loop clusters: (c) *A. thaliana* M-loop; (d) *A. thaliana* M-loop stabilized by IVM; (g) *H. contortus* M-loop; (h) *H. contortus* M-loop stabilized by IVM.

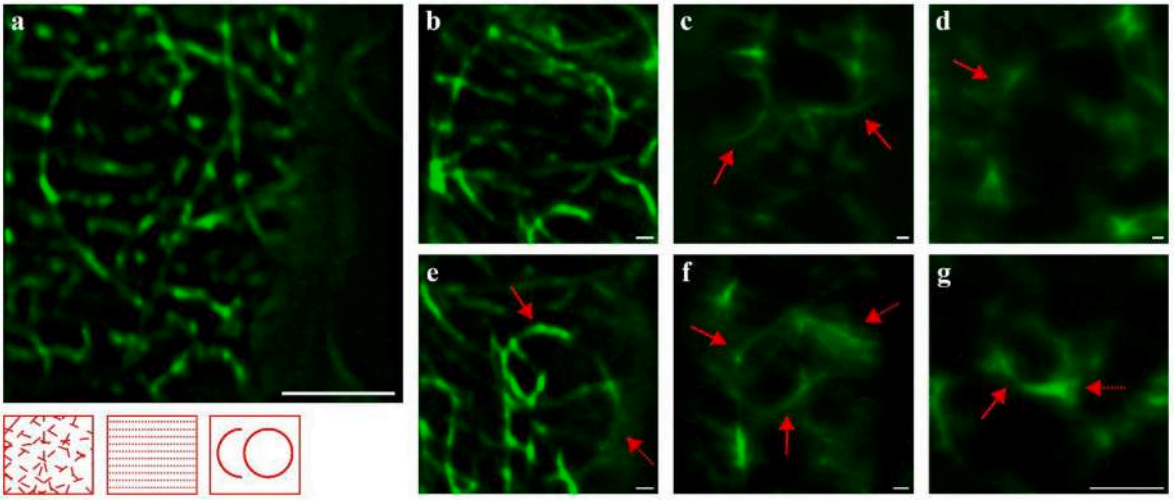

Fig. 10. MT cyclic assemblies in epidermal cells of *A. thaliana gfp-map4* line after 1 h of 250 μg mL^{-1} IVM treatment: (a) cell division zone; (b, e) root apex; (c, d) elongation zone; (f, g) transition zone. Bar = 3 μm.

IVM concentrations are higher than typically found in soil (Iglesias et al., 2018), it should be taken into account that the concentration of IVM in a specific zone depends on various factors: for example, administered doses of the IVM, biotransformation of IVM in the body of treated animals and, as a result, the amount of the drug in faeces, etc. In addition, susceptibility to IVM varies among the few plant species studied to date; for example, as mentioned earlier, Vokřál et al. (2019) reported inhibition of root growth in *S. alba* seedlings at an IVM concentration of 0.044 μg mL^{-1}, which is much lower than concentrations used in our study. Therefore, it is important to investigate the effect of IVM on the growth and development of other plant species, as well as to use model lines to elucidate the mode of action of IVM and search for its potential targets in plant cells.

Since plant growth (cell division and cell elongation) and development (cell differentiation) are directly dependent on the correct functioning of the cytoskeleton, and in particular microtubules, we studied how the IVM affects MTs in *A. thaliana* cells. Previously it was shown that IVM has a stabilizing effect on the *H. contortus* MTs (Ashraf et al. (2015a, 2015b). The results of surface plasmon resonance and equilibrium dialysis (Ashraf et al., 2015a), indicate that IVM competes with taxol for the same binding site in *H. contortus* isotype 1 recombinant tubulin, laying the foundations for this research. Considering tubulin conservancy, and particularly the similarity of taxane site, IVM interactions with MTs of *A. thaliana* primary root cells were studied using confocal laser scanning microscopy. For visualization of MTs in living cells we used the transgenic *A. thaliana* line expressing the fused gene *gfp-map4* (Marc et al., 1998; Mathur and Chua, 2000), and also *A. thaliana* line expressing fused *gfp-tua6* gene to confirm our findings with MT organization after IVM treatment in both reporter systems. Consequently, the disruption of cortical network, MT curving, and appearance of bundled MTs after treatment with 250 μg mL^{-1} IVM were observed (Fig. 2f,k,p; Fig. 3f,n). Since Ashraf et al. (2015a) reported that competition between taxol and IVM for taxane sites, the IVM effect on plant MTs can be compared with the taxol effect as a traditional MT stabilizing agent. Taxol influence on arrangements of plant MTs has been extensively studied in the last two decades (Mathur and Chua, 2000; Korolev et al., 2005). Among the common effects of taxol treatment are loss of MT orientations and MT stabilization, which subsequently increases the number of MTs, causes longitudinal alignment, and assembling into characteristic thick bundles.

Similar to taxol, loss of MT orientations was observed frequently after IVM treatment in both (*gfp-map4* and *gfp-tua6)* lines of *A. thaliana* and confirmed quantitatively (Fig. 4b, c, d; Fig. 5d). Although cross-linked bundling of MTs prevails in IVM-treated cells (Fig. 10a–g), short alignment and bundling of MTs were also found (Fig. 2o; Fig. 5c). Despite the disrupting effects of IVM on interphase MTs, such MT figures as the mitotic spindles were visualized in meristematic cells of IVM-treated seedlings of *A. thaliana gfp-map4* line (Fig. 2 l, m). Also, it should be noted that we have previously found that both populations of MTs (i.e., cortical and mitotic) may differ in their sensitivity to certain antimitotic drugs (Yemets et al., 2008). Moreover, although it was possible to study the IVM effect on MT arrangements in epidermal cells of *gfp-tua6* root apex (Fig. 5), in cells of other root zones a signal was either absent or too weak for MTs to be distinguished in surrounding noise, which is explained by cell-specific expression of *TUA6* gene (Ueda et al., 1999). Despite the *gfp-tua6* line of *A. thaliana* is generally considered a more suitable model for studying MT arrangements as compared to the *gfp-map4* line, in which GFP protein is fused with the microtubule-binding domain of mammalian MAP4 (Marc et al., 1998), the lack of reporter signal in cells of most root zones prevent the use of *A. thaliana* line expressing *gfp-tua6* chimeric gene as a viable alternative model for studying MT organization in living cells of primary roots.

Based on the recent advances in understanding MT dynamics, MT structure is significantly dependent on the conformation of M-loops in α- and β-tubulin (Debs et al., 2020). Since M-loop also plays a key role in MT stabilization, the impact of taxane site effectors on MT structure must be significant. Based on the article by Debs et al. (2020), an IVM influence on MT structure can include variation in the number of protofilaments, MT wall distortion, and structural deformations occurring during MT polymerization. Further, depending on their structures, taxane site ligands can cause different changes in M-loop conformation, which means that the effect on MT structure can be different for structurally distinct compounds such as IVM and taxol. Finally, the effect on MT structure can vary depending on IVM binding to already polymerized or free tubulin subunits, which was previously reported for taxol-treated MTs (Kellogg et al., 2017). In this way, differences in MT curving and disruptions among different MT populations treated with IVM can be explained. Although IVM interactions with M-loop were predicted by Ashraf et al. (2015a) based on homology modelling and molecular docking, no MD verification of IVM interaction with the taxane site has been made and no detailed explanation of binding has been reported yet.

Since tubulin from plant sources is much more difficult to polymerize *in vitro* than tubulin from animal sources (Xu et al., 2005) to perform polymerization assay on IVM binding to plant tubulin, such interaction can also be predicted computationally using *in silico* methods based on previously validated experimental data demonstrating competitive (with taxol) binding of IVM to recombinant *H. contortus* β1-tubulin (Ashraf et al., 2015a) and porcine tubulin (Ashraf et al., 2015b). Given the conservation of tubulin and, in particular, the conservation of taxane site (e.g., multiple sequence alignment results), we can predict that IVM interaction with β-tubulin of *A. thaliana* is possible.

In this research, IVM interactions with taxane sites of *A. thaliana* and *H. contortus* β1-tubulins were studied using 100 ns MD with original AlphaFold models. Analysing the most common conformations of the collected ensembles of complexes, it was found that the taxane site of β1-tubulin of *H. contortus* has a higher affinity for IVM, which explains the high concentration of IVM at which its effect on *A. thaliana* MTs was observed. The distinction in effective concentrations can also be explained by possible differences in IVM translocation inside *A. thaliana* cells and its binding to other molecular targets with higher affinity. Since both IVM-tubulin complexes have passed the verification with 100 ns MD, the obtained results allow us to confirm IVM binding to β-tubulin. According to the latter, the IVM macrocycle, spiroketal and benzofuran groups play a key role in interactions with tubulin. Since Ashraf et al. (2015b) previously reported that the structurally related compound moxidectin, which lacks the disaccharide group, increases polymerization rates of *H. contortus* tubulin in a similar manner to IVM, this allows us to assume that disaccharide group may also not be necessary for the molecular mechanics of IVM stabilizing effect on MTs. Another fact that was considered during the spatial reconstruction of the proposed binding site is the experimental evidence of the affinity of taxane site second sub cavity for benzene ring, which was recently revealed crystallographically by the results of fragment screening of N-methyl-2-(methylsulfonyl)aniline and N-ethyl-2-fluoro-4-(methylsulfonyl)aniline to mammalian tubulin (PDB id: 5S4N, 5S4M) performed by Mühlethaler et al. (2021). Despite the structure of IVM lacking completely planar rings, a similarity in stereochemical properties of cyclohexene and benzene rings makes the second subcavity of the taxane site a possible location of the IVM benzofuran group. Given the absence of correlation between IVM h-bonds and polar contacts established with residues of M-loop and its stabilizing effect on M-loop conformation, the effect can be rather allosteric than related to IVM direct interactions with this structure element. Also, as it was found using MSA, the M-loop sequence varies significantly for *A. thaliana* and *H. contortus* β1-tubulin and even inside the isotypes of *A. thaliana* β-tubulin (Fig. 6). Despite this, the overall conservation of taxane site residues among eight β-tubulin isotypes revealed by MSA allows us to assume that IVM can also bind to microtubules in cells of other tissues of *A. thaliana*.

5. Conclusions

According to the results of our investigation, IVM impacts negatively on the growth and root morphology of *A. thaliana* seedlings at studied concentrations. IVM dramatically disturbs MTs in epidermal cells of the root tip, transition and elongation zones of *A. thaliana*. In particular, IVM treatment led to the disruption of MT organization, their bundling and assembling into circular formations. On the contrary, no significant effect of IVM on the MTs was observed in cells of the differentiation zone. For confirmations of the specific interaction of IVM with plant MTs 3-D model of its binding site in *A. thaliana* β1-tubulin was developed and verified by using molecular dynamics simulation based on earlier prediction of IVM binding to the taxane site of β1-tubulin of *Haemonchus contortus*. According to the results of molecular modelling, the IVM effect on MTs can be explained by IVM-induced changes in the conformation of the M-loop, which is known to be the key element in MT wall dynamics. We also confirmed, that similar to other MT stabilizing agents ivermectin binding causes M-loop stabilization in β-tubulin, which can lead to the enhancement of lateral contacts between subunits of adjacent protofilaments preventing MT depolymerization. Considering these findings, it seems that β-tubulin of *A. thaliana* represents an important intracellular target for IVM action.

Funding

This work was financially supported by the National Academy of Sciences of Ukraine (project registration number #0120U103109, 2020–2022, and budget theme, code #6541030).

Author contributions

Yevhen Kustovskiy: Investigation, Methodology, Validation, Writing – original draft. Pavel Karpov: Investigation, Methodology, Validation. Yaroslav Blume: Methodology, Review, and critical remarks. Alla Yemets: Methodology, Conceptualization, Supervision, Data Analysis, Article Writing, and Editing.

Ethical approval

Not applicable.

Consent to participate

Not applicable.

Code availability

Not applicable.

Declaration of competing interest

The authors declare that they have no known competing financial interests or personal relationships that could have appeared to influence the work reported in this paper.

Data availability

All data analyzed during this study are included in this published article.

Acknowledgements

The study was carried out using CCDC GOLD software, kindly provided by the Cambridge Crystallographic Data Center (CCDC) as part of the Frank H. Allen International Research and Education Program (FAIRE) grant ID: 21554, and BioSolveIT SeeSAR software, kindly provided by the Gloria Kraschinski (Senior Account Manager at BioSolveIT GmbH).

References

Abraham, M.J., Murtola, T., Schulz, R., Pall, S., Smith, J.C., Hess, B., Lindahl, E., 2015. GROMACS: high performance molecular simulations through multi-level parallelism from laptops to supercomputers. SoftwareX 1–2, 19–25. https://doi.org/10.1016/j.softx.2015.06.001.

Ashraf, S., Beech, R.N., Hancock, M.A., Prichard, R.K., 2015a. Ivermectin binds to *Haemonchus contortus* tubulins and promotes stability of microtubules. Int. J. Parasitol. 45 (9–10), 647–654. https://doi.org/10.1016/j.ijpara.2015.03.010.

Ashraf, S., Mani, T., Beech, R., Prichard, R., 2015b. Macrocyclic lactones and their relationship to the SNPs related to benzimidazole resistance. Mol. Biochem. Parasitol. 201 (2), 128–134. https://doi.org/10.1016/j.molbiopara.2015.07.007.

Ballesteros, C., Tritten, L., O'Neill, M., Burkman, E., Zaky, W.I., Xia, J., Moorhead, A., Williams, S.A., Geary, T.G., 2016. The effects of ivermectin on *Brugia malayi* females *in vitro*: a transcriptomic approach. PLoS Neglected Trop. Dis. 10 (8), 1–19. https://doi.org/10.1371/journal.pntd.0004929.

Blume, Y.B., Krasylenko, Y.A., Demchuk, O.M., Yemets, A.I., 2013. Tubulin tyrosine nitration regulates microtubule organization in plant cells. Front. Plant Sci. 4 (530), 1–14. https://doi.org/10.3389/fpls.2013.00530.

Blume, Y., Yemets, A., Sheremet, Y., Nyporko, A., Sulimenko, V., Sulimenko, T., Draber, P., 2010. Exposure of beta-tubulin regions defined by antibodies on a *Arabidopsis thaliana* microtubule protofilament model and in the cells. BMC Plant Biol. 10, 1–10. https://doi.org/10.1186/1471-2229-10-29.

Chen, I.S., Kubo, Y., 2018. Ivermectin and its target molecules: shared and unique modulation mechanisms of ion channels and receptors by ivermectin. J. Physiol. 596 (10), 1833–1845. https://doi.org/10.1113/jp275236.

Darden, T., York, D., Pedersen, L., 1993. Particle mesh Ewald: an *N*·log(*N*) method for Ewald sums in large systems. J. Chem. Phys. 98 (12), 10089–10092. https://doi.org/10.1063/1.464397.

Daura, X., Gademann, K., Jaun, B., Seebach, D., van Gunsteren, W.F., Mark, A.E., 1999. Peptide folding: when simulation meets experiment. Angew. Chem. Int. Ed. 38 (1/2), 236–240. https://doi.org/10.1002/(SICI)1521-3773(19990115)38:1/2%3C236::AID-ANIE236%3E3.0.CO;2-M.

Debs, G.E., Cha, M., Liu, X., Huehn, A.R., Sindelar, C.V., 2020. Dynamic and asymmetric fluctuations in the microtubule wall captured by high-resolution cryoelectron microscopy. Proc. Natl. Acad. Sci. U.S.A. 117 (29), 16976–16984. https://doi.org/10.1073/pnas.2001546117.

de Souza, R.B., de Souza, C.P., Guimarães, J.R., 2022. Environmentally realistic concentrations of eprinomectin induce phytotoxic and genotoxic effects in *Allium cepa*. Environ. Sci. Pollut. Res. Int. 29 (53), 80983–80993. https://doi.org/10.1007/s11356-022-21403-7.

Eng, J.K., Blackhall, W.J., Osei-Atweneboana, M.Y., Bourguinat, C., Galazzo, D., Beech, R.N., Unnasch, T.R., Awadzi, K., Lubega, G.W., Prichard, R.K., 2006. Ivermectin selection on beta-tubulin: evidence in *Onchocerca volvulus* and *Haemonchus contortus*. Mol. Biochem. Parasitol. 150 (2), 229–235. https://doi.org/10.1016/j.molbiopara.2006.08.007.

González Canga, A., Sahagún Prieto, A.M., José Diez Liébana, M., Martínez, N.F., Vega, M.S., Vieitez, J.J., 2009. The pharmacokinetics and metabolism of ivermectin in domestic animal species. Vet. J. 179 (1), 25–37. https://doi.org/10.1016/j.tvjl.2007.07.011.

Huang, J., MacKerell Jr., A.D., 2013. CHARMM36 all-atom additive protein force field: validation based on comparison to NMR data. J. Comput. Chem. 34 (25), 2135–2145. https://doi.org/10.1002/jcc.23354.

Humphrey, W., Dalke, A., Schulten, K., 1996. VMD: visual molecular dynamics. J. Mol. Graph. 14 (1), 33–38. https://doi.org/10.1016/0263-7855(96)00018-5.

Iglesias, L.E., Saumell, C., Sagüés, F., Sallovitz, J.M., Lifschitz, A.L., 2018. Ivermectin dissipation and movement from feces to soil under field conditions. J. Environ. Sci. Health B. 53 (1), 42–48. https://doi.org/10.1080/03601234.2017.1371554.

Jones, G., Willett, P., Glen, R.C., Leach, A.R., Taylor, R., 1997. Development and validation of a genetic algorithm for flexible docking. J. Mol. Biol. 267 (3), 727–748. https://doi.org/10.1006/jmbi.1996.0897.

Jumper, J., Evans, R., Pritzel, A., Green, T., Figurnov, M., Ronneberger, O., Tunyasuvunakool, K., Bates, R., Žídek, A., Potapenko, A., et al., 2021. Highly accurate protein structure prediction with AlphaFold. Nature 596 (7873), 583–589. https://doi.org/10.1038/s41586-021-03819-2.

Karpov, P.A., Brytsun, V.M., Rayevsky, A.V., Demchuk, O.M., Pydiura, N.O., Ozheredov, S.P., Samofalova, D.A., Spivak, S.I., Yemets, A.I., Kalchenko, V.I., Blume, YaB., 2015. High-throughput screening of new antimitotic compounds based on CSLabGrid virtual organization. Sci. Innovat. 11 (1), 85–93. https://doi.org/10.15407/scin11.01.092.

Kellogg, E.H., Hejab, N.M.A., Howes, S., Northcote, P., Miller, J.H., Díaz, J.F., Downing, K.H., Nogales, E., 2017. Insights into the distinct mechanisms of action of taxane and non-taxane microtubule stabilizers from cryo-EM structures. J. Mol. Biol. 429 (5), 633–646. https://doi.org/10.1016/j.jmb.2017.01.001.

Korb, O., Stützle, T., Exner, T.E., 2009. Empirical scoring functions for advanced protein-ligand docking with PLANTS. J. Chem. Inf. Model. 49 (1), 84–96. https://doi.org/10.1021/ci800298z.

Korolev, A.V., Chan, J., Naldrett, M.J., Doonan, J.H., Lloyd, C.W., 2005. Identification of a novel family of 70 kDa microtubule-associated proteins in Arabidopsis cells. Plant J. 42 (4), 547–555. https://doi.org/10.1111/j.1365-313x.2005.02393.x.

Laing, R., Gillan, V., Devaney, E., 2017. Ivermectin - old drug, new tricks? Trends Parasitol. 33 (6), 463–472. https://doi.org/10.1016/j.pt.2017.02.004.

Langhansová, L., Navrátilová, M., Skálová, L., Moťková, K., Podlipná, R., 2021. The effect of the manure from sheep treated with anthelmintics on clover (*Trifolium pratense*). Agronomy 11, 1–14. https://doi.org/10.3390/agronomy11091892.

Marc, J., Granger, C.L., Brincat, J., Fisher, D.D., Kao, Th, McCubbin, A.G., Cyr, R.J., 1998. A GFP-MAP4 reporter gene for visualizing cortical microtubule rearrangements in living epidermal cells. Plant Cell 10 (11), 1927–1940. https://doi.org/10.1105/tpc.10.11.1927.

Martin, R.J., Robertson, A.P., Choudhary, S., 2020. Ivermectin: an anthelmintic, an insecticide, and much more. Trends Parasitol. 37 (1), 48–64. https://doi.org/10.1016/j.pt.2020.10.005.

Mathur, J., Chua, N.H., 2000. Microtubule stabilization leads to growth reorientation in Arabidopsis trichomes. Plant Cell 12 (4), 465–477. https://doi.org/10.1105/tpc.12.4.465.

Mooij, W.T., Verdonk, M.L., 2005. General and targeted statistical potentials for protein-ligand interactions. Proteins 61 (2), 272–287. https://doi.org/10.1002/prot.20588.

Mühlethaler, T., Gioia, D., Prota, A.E., Sharpe, M.E., Cavalli, A., Steinmetz, M.O., 2021. Comprehensive binding analysis of sites in tubulin. Angew. Chem., Int. Ed. Engl. 60 (24), 13331–13342. https://doi.org/10.1002/anie.202100273.

Navrátilová, M., Raisová Stuchlíková, L., Skálová, L., Szotáková, B., Langhansová, L., Podlipná, R., 2020. Pharmaceuticals in environment: the effect of ivermectin on ribwort plantain (*Plantago lanceolata* L.). Environ. Sci. Pollut. Res. Int. 27 (25), 31202–31210. https://doi.org/10.1007/s11356-020-09442-4.

Sasaki, T., Fukuda, H., Oda, Y., 2017. CORTICAL MICROTUBULE DISORDERING1 is required for secondary cell wall patterning in xylem vessels. Plant Cell 29 (12), 3123–3139. https://doi.org/10.1105/tpc.17.00663.

Schindelin, J., Arganda-Carreras, I., Frise, E., Kaynig, V., Longair, M., Pietzsch, T., Preibisch, S., Rueden, C., Saalfeld, S., Schmid, B., et al., 2012. Fiji: an open-source platform for biological-image analysis. Nat. Methods 9 (7), 676–682. https://doi.org/10.1038/nmeth.2019.

Schneider, N., Lange, G., Hindle, S., Klein, R., Rarey, M., 2013. A consistent description of HYdrogen bond and DEhydration energies in protein-ligand complexes: methods behind the HYDE scoring function. J. Comput. Aided Mol. Des. 27 (1), 15–29. https://doi.org/10.1007/s10822-012-9626-2.

Schrödinger Release, 2022-1, 2022. Maestro, Schrödinger, LLC. New York, NY.

SeeSAR version 12.1.0, 2023. BioSolveIT GmbH. Sankt Augustin, Germany. www.biosolveit.de/SeeSAR.

Syslová, E., Landa, P., Navrátilová, M., Stuchlíková, L.R., Matoušková, P., Skálová, L., Szotáková, B., Vaněk, T., Podlipná, R., 2019. Ivermectin biotransformation and impact on transcriptome in *Arabidopsis thaliana*. Chemosphere 234, 528–535. https://doi.org/10.1016/j.chemosphere.2019.06.102.

Ueda, K., Matsuyama, T., Hashimoto, T., 1999. Visualization of microtubules in living cells of transgenic *Arabidopsis thaliana*. Protoplasma 206, 201–206. https://doi.org/10.1007/BF01279267.

Vokřál, I., Šadibolová, M., Podlipná, R., Lamka, J., Prchal, L., Sobotová, D., Lokvencová, K., Szotáková, B., Skálová, L., 2019. Ivermectin environmental impact: excretion profile in sheep and phytotoxic effect in Sinapis alba. Ecotoxicol. Environ. Saf. 169, 944–949. https://doi.org/10.1016/j.ecoenv.2018.11.097.

Volkamer, A., Griewel, A., Grombacher, T., Rarey, M., 2010. Analyzing the topology of active sites: on the prediction of pockets and subpockets. J. Chem. Inf. Model. 50 (11), 2041–2052. https://doi.org/10.1021/ci100241y.

Volkamer, A., Kuhn, D., Rippmann, F., Rarey, M., 2012. DoGSiteScorer: a web server for automatic binding site prediction, analysis and druggability assessment. Bioinformatics 28 (15), 2074–2075. https://doi.org/10.1093/bioinformatics/bts310.

Waterhouse, A.M., Procter, J.B., Martin, D.M., Clamp, M., Barton, G.J., 2009. Jalview Version 2–a multiple sequence alignment editor and analysis workbench. Bioinformatics 25 (9), 1189–1191. https://doi.org/10.1093/bioinformatics/btp033.

Xu, C.-H., Huang, S.-J., Yuan, M., 2005. Dimethylsulfoxide is feasible for plant tubulin assembly *in vitro*: a comprehensive analysis. J. Integr. Plant Biol. 47 (4), 457–466.

Yemets, A., Stelmakh, O., Blume, YaB., 2008. Effects of the herbicide isopropyl-*N*-phenyl carbamate on microtubules and MTOCs in lines of *Nicotiana sylvestris* resistant and sensitive to its action. Cell Biol. Int. 32 (6), 623–629. https://doi.org/10.1016/j.cellbi.2008.01.012.

Zoete, V., Cuendet, M.A., Grosdidier, A., Michielin, O., 2011. SwissParam: a fast force field generation tool for small organic molecules. J. Comput. Chem. 32 (11), 2359–2368. https://doi.org/10.1002/jcc.21816.